

Non-Fermi liquid, unscreened scalar chirality and parafermions in a frustrated tetrahedron Anderson model

K. Hattori and H. Tsunetsugu
Institute for Solid State Physics, University of Tokyo,
Kashiwanoha 5-1-5, Kashiwa, Chiba 277-8581, Japan
 (Dated: February 20, 2018)

We investigate a four-impurity Anderson model where localized orbitals are located at vertices of a regular tetrahedron and find a novel fixed point in addition to the ordinary Fermi liquid phase. That is characterized by unscreened scalar chirality of a tetrahedron. In this phase, parafermions emerges in the excitation spectrum and quasiparticle mass diverges as $1/|T \ln^3 T|$ at low temperatures (T). The diverging effective mass is a manifestation of singular Fermi liquid states as in the underscreened Kondo problem. Between the two phases, our Monte Carlo results show the existence of a non Fermi liquid critical point where the Kondo effects and the intersite antiferromagnetic interactions are valanced. Singular behaviors are prominent in the dynamics and we find that the frequency dependence of the self-energy is the marginal Fermi liquid like $-\text{Im}\Sigma \sim |\omega|$.

PACS numbers: 72.15.Qm, 74.40.Kb, 75.10.Jm

I. INTRODUCTION

The Kondo problem of multiple impurities has attracted much attention since the pioneering work of the two-impurity system about 25 years ago.¹ The presence of two competing energy scales, the Kondo temperature and the intersite exchange interaction, provides a nice play ground of quantum phase transition at zero temperature. Around the quantum critical point, non Fermi liquid (NFL) behaviors emerge and thermodynamic quantities and their dynamics exhibit singular temperature dependence. These physics have a connection to quantum criticality in heavy fermion systems² and, thus, understanding much simpler cluster problems is a key to capturing the nature of more complicated problems.

Quantum fluctuations in such strongly correlated systems can be controlled by tuning geometrical frustration. This is the case not only in spin systems but also in itinerant electron systems and the frustration leads to novel ground states such as spin liquid states.³ As for the Kondo problem, frustration can be implemented by introducing a cluster of multiple impurities, and also controlling its geometry. When the cluster is frustrated, its ground state is degenerate due to nonmagnetic degrees of freedom. In the simplest case where the cluster is a triangle,⁴ the ground state is degenerate in the spin and the chirality sectors. Its Kondo problem was studied by the combination of the numerical renormalization group (NRG) and boundary conformal field theory (BCFT),⁵ and also by the continuous time quantum Monte Carlo (CTQMC) method⁶ and the renormalization group (RG).⁷ It has been established that the frustration leads to a NFL phase. This phase is stable against perturbations that keep the triangular symmetry such as magnetic fields and particle-hole asymmetry,⁵ which contrasts with the unstable NFL in the two-impurity case.¹

This paper reports extensive analysis on a minimal three-dimensional cluster problem with geometrical frustration, the Kondo problem of a regular tetrahedron.

Tetrahedrons are simplex, *i.e.*, the basic structure for three dimensional “frustrated” materials such as pyrochlore and spinel compounds. The result presented here would be helpful for further studies on the lattice problem in addition to the standpoint as a fundamental model analysis.

This paper is organized as follows. In Sec. II, we introduce a microscopic model for four impurities. We analyze its two stable fixed points in Sec. III, with emphasis on an unscreened phase. Section IV is devoted to clarifying the global phase diagram and discussions about a critical point between the two stable fixed points. Finally, we summarize the present results in Sec. V

II. MODEL

We first introduce a four-impurity Anderson model, in which localized s -wave orbitals are located at vertices of a regular tetrahedron and hybridize with a conduction band:

$$\begin{aligned} \mathcal{H} = & \sum_{\sigma} \int \frac{d\mathbf{k}}{(2\pi)^3} \epsilon_{\mathbf{k}} \psi_{\mathbf{k}\sigma}^{\dagger} \psi_{\mathbf{k}\sigma} + \sum_{i\sigma} \epsilon d_{i\sigma}^{\dagger} d_{i\sigma} \\ & + V_0 \sum_{i\sigma} \int \frac{d\mathbf{k}}{\sqrt{(2\pi)^3}} (e^{i\mathbf{k}\cdot\mathbf{x}_i} d_{i\sigma}^{\dagger} \psi_{\mathbf{k}\sigma} + \text{h.c.}) \\ & - t \sum_{i,j} d_{i\sigma}^{\dagger} d_{j\sigma} + U \sum_i n_{i\uparrow} n_{i\downarrow}, \end{aligned} \quad (1)$$

where $\psi_{\mathbf{k}\sigma}^{\dagger}$ creates a conduction electron with wave vector \mathbf{k} and spin σ , $d_{i\sigma}^{\dagger}$ creates a localized electron at position \mathbf{x}_i ($i = 1, 2, 3$ or 4), $n_{i\sigma} = d_{i\sigma}^{\dagger} d_{i\sigma}$ and other parameters are conventional ones. We also introduce the d -electron spin operator \mathbf{S}_i at \mathbf{x}_i , for later use.

It is useful to transform ψ to partial waves¹ that couple with d electrons. In the new basis, Hamiltonian (1) is

written as

$$\mathcal{H} = \sum_{\alpha\sigma} \int dk \left[\epsilon_k \psi_{k\alpha\sigma}^\dagger \psi_{k\alpha\sigma} + V_\alpha (d_{\alpha\sigma}^\dagger \psi_{k\alpha\sigma} + \text{h.c.}) \right] + \sum_{\alpha} \epsilon_\alpha d_{\alpha\sigma}^\dagger d_{\alpha\sigma} + U \text{ terms}, \quad (2)$$

where the orbital index α runs over four channels: (s, x, y, z) . The orbital $s(x, y, z)$ is the basis of the $A_1(T_2)$ representation in the T_d point group. The dependence of V_α on wave number $k=|\mathbf{k}|$ is ignored and replaced by the value at the Fermi wave number k_F : $V_s=V[1+3\sin(k_F a)/k_F a]^{1/2}$ and $V_{x,y,z}=V[1-\sin(k_F a)/k_F a]^{1/2}$, with $a=|\mathbf{x}_1-\mathbf{x}_2|$ being the impurity-impurity distance. V is a parameter proportional to V_0 . The orbital energy is given as $\epsilon_s=\epsilon-3t$ and $\epsilon_{x,y,z}=\epsilon+t$. The new basis for d electrons is given by

$$d_{\alpha\sigma} = \frac{1}{2} \sum_i (\mathbf{f}^\alpha)_i d_{i\sigma}, \quad (3)$$

with $\mathbf{f}^s=(1, 1, 1, 1)$, $\mathbf{f}^x=(1, -1, 1, -1)$, $\mathbf{f}^y=(1, -1, -1, 1)$, and $\mathbf{f}^z=(1, 1, -1, -1)$, and similar expressions for the conduction electrons. The bandwidth is set to $2D$ centered at the Fermi level and the density of states is set to constant $\rho=1/2D$ for all $\psi_{k\alpha\sigma}$.

III. TWO STABLE FIXED POINTS

First, we investigate two stable fixed points in the Kondo regime, where the d electron is nearly half filling $\sum_\sigma n_{i\sigma}\sim 1$. Note that there are two competing energy scales. One is the on-site Kondo energy $T_K\sim D \exp(-|\epsilon|/4\rho V_0^2)$. The other is the inter-site exchange interaction J , which includes superexchange and Ruderman-Kittel-Kasuya-Yosida (RKKY) interactions. For $T_K\gg J$, the Fermi liquid (FL) fixed point is stable, where each d electron forms a spin singlet with conduction electrons. In the opposite limit, $J\gg T_K$, four localized spins form spin singlets with a nonmagnetic double degeneracy: the E representation in the T_d group. The two states in the doublet can be characterized as eigenstates of the scalar chirality (SC)

$$\chi = \mathbf{S}_i \cdot (\mathbf{S}_j \times \mathbf{S}_k), \quad (4)$$

with $i \neq j \neq k$.⁸ The question is what happens when the interactions are switched on between the chirality doublet and conduction electrons? We show that conduction electrons cannot screen this doublet. Between the two stable fixed points, there exists a critical point as shown in Fig. 1, and we discuss this in Sec. IV.

A. Unscreened phase

1. An effective model

In order to investigate the limit $J \gg T_K$, we first derive an effective model of the local ground-state doublet. We

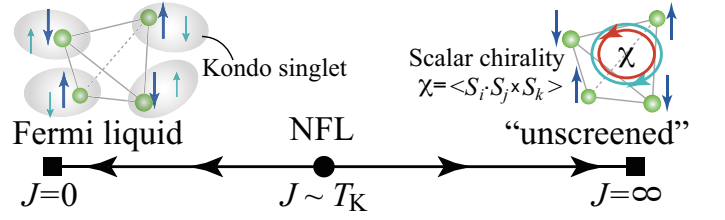


FIG. 1: (Color online) Schematic renormalization flow in the Kondo regime as a function of intersite exchange interaction J .

represent it by a pseudospin 1/2, whose bases are

$$|\uparrow\rangle = \frac{1}{2}(1 + \hat{I})(|\uparrow\uparrow\uparrow\rangle - |\uparrow\downarrow\uparrow\rangle), \quad (5)$$

$$|\downarrow\rangle = \frac{1}{\sqrt{3}}(1 + \hat{I})[|\uparrow\uparrow\downarrow\rangle - \frac{1}{2}(|\uparrow\downarrow\uparrow\rangle + |\uparrow\downarrow\downarrow\rangle)]. \quad (6)$$

Here, $|\sigma_1\sigma_2\sigma_3\sigma_4\rangle$ represents a state with the z component of spin σ_i at site i and \hat{I} is the spin inversion operator. The effective model is strongly restricted by its symmetry. Since possible operators of the local E doublet are $E\otimes E=A_1\oplus A_2\oplus E$, nontrivial couplings are those in the A_2 and E sectors. Taking into account the classifications for the conduction electron bilinear operators, $T_2\otimes T_2=A_1\oplus E\oplus T_1\oplus T_2$, $A_1\otimes A_1=A_1$, and $A_1\otimes T_2=T_2$, only a coupling in the E sector is possible:

$$\mathcal{H}_{\text{int}} = g(\tau^z \mathcal{Q} + \tau^x \mathcal{T}), \quad (7)$$

where $g \propto t|V_x|^2/|\epsilon|^2$ for $U\rightarrow\infty$ and (τ^z, τ^x) are the spin-1/2 operators for the pseudospin with the E representation. The conduction electron parts,

$$\mathcal{Q} \equiv \frac{1}{\sqrt{6}}(\mathcal{N}_x + \mathcal{N}_y - 2\mathcal{N}_z), \quad (8)$$

$$\mathcal{T} \equiv \frac{1}{\sqrt{2}}(\mathcal{N}_y - \mathcal{N}_x), \quad (9)$$

are the local orbital density with

$$\mathcal{N}_\alpha \equiv \sum_\sigma \int dk dk' \psi_{k\alpha\sigma}^\dagger \psi_{k'\alpha\sigma}. \quad (10)$$

They are the E representation and the “quadrupole” operator with $[\mathcal{Q}, \mathcal{T}] = 0$. This commutativity distinguishes Eq. (7) from a conventional quadrupole Kondo model⁹ and leads novel behaviors as discussed below. Note that \mathcal{N}_s does not couple and the SC is represented by $\chi=\sqrt{3}\tau^y$, which is the A_2 representation and cannot appear in the Hamiltonian.

2. Perturbative renormalization group

Next, we analyze the effective Hamiltonian (7) by RG. It is remarkable that the one-loop order term vanishes and the leading order is the two-loop level, and the RG equation is

$$D \frac{\partial g}{\partial D} = \frac{1}{2} \rho^2 g^3. \quad (11)$$

The absence of $O(g^2)$ terms in the RG equation is traced in $[\mathcal{Q}, \mathcal{T}] = 0$. Solving the RG equation, we obtain

$$\rho g_{\text{eff}} = \frac{1}{\sqrt{\ln(T^*/D_{\text{eff}})}}, \quad (12)$$

with $T^* \equiv D \exp[1/(\rho g)^2]$ as the effective bandwidth is decreased to D_{eff} . This asymptotic logarithmic form is similar to that in the underscreened Kondo model¹⁰ aside from the extra power 1/2. Thus, the coupling constant approaches zero with lowering temperature (energy). The impurity degrees of freedom cannot be screened and there remains a residual entropy $\ln 2$. The pseudospin susceptibility has the Curie like temperature dependence

$$\chi_{zz} \equiv \int_0^{1/T} \langle T_\tau \tau^z(\tau) \tau^z(0) \rangle d\tau \sim T^{-1}, \quad (13)$$

where T_τ represents time-ordering. Summing up the leading logarithmic terms, we find that the impurity specific heat coefficient C_{imp}/T diverges as

$$\frac{C_{\text{imp}}}{T} \sim \frac{1}{T \ln^3(T^*/T)}. \quad (14)$$

This means a diverging effective mass, and the power 3 is different from that in ‘‘singular’’ Fermi liquid states.¹⁰

3. Boundary conformal field theory and numerical renormalization group analysis

The presence of the unscreened phase is explicitly demonstrated in our NRG¹¹ calculations. Energy levels have degeneracy expected for their quantum numbers (see below) plus an additional factor 2. This double degeneracy is a manifestation of the unscreened SC. The quantum numbers of each level consist of three parts: total charge Q , spin j , and the orbital part. The energies and the quantum numbers are in complete agreement with the prediction below derived via ‘‘phase shift’’ in the orbital sector in the BCFT language,¹² assuming an unscreened SC. This confirms that the unscreened local object in this phase is a SC, or equivalently different configurations of two spin-singlet pairs.⁸

Let us explain our BCFT analysis. We first introduce a conformal embedding suitable to Eq. (7). The free Hamiltonian is represented by in addition to the global U(1) charge current, the spin and orbital

currents following the Kac-Moody algebra $SU(2)_3$ and $SU(3)_2$, respectively. One possible conformal embedding is $U(1) \otimes SU(2)_3 \otimes SU(3)_2$, and the energy eigenvalues of the free Hamiltonian are represented as

$$E^0 = \frac{\pi v_F}{l} \left[\frac{Q^2}{12} + \frac{j(j+1)}{5} + \frac{c_{SU(3)}}{5} + \text{integer} \right], \quad (15)$$

where we have defined the effective one-dimensional space in $[-l, l]$, v_F is the Fermi velocity, and $c_{SU(3)}$ is the eigenvalue of the Casimir operator in the SU(3) sector: $c_{SU(3)} = 0$ for **1**, $c_{SU(3)} = 4/3$ for **3** and $\bar{\mathbf{3}}$, $c_{SU(3)} = 10/3$ for **6** and $\bar{\mathbf{6}}$, and $c_{SU(3)} = 3$ for **8**.

The interaction (7) preserves each of the charges in the T_2 orbital separately, although it breaks the orbital SU(3) symmetry. This means there remains two conserved U(1) charges in the orbital sector:

$$\bar{Q} \equiv \frac{1}{\sqrt{6}} (\bar{N}_x + \bar{N}_y - 2\bar{N}_z), \quad (16)$$

$$\bar{T} \equiv \frac{1}{\sqrt{2}} (\bar{N}_y - \bar{N}_x), \quad (17)$$

with

$$\bar{N}_\alpha \equiv \sum_\sigma \int dk \psi_{k\alpha\sigma}^\dagger \psi_{k\alpha\sigma}. \quad (18)$$

Note that the total orbital charge \bar{N}_α differs from the local density \mathcal{N}_α and $Q = \sum_\alpha \bar{N}_\alpha$. Factorized out with these two U(1) charges, the CFT for the remaining orbital part $SU(3)_2/[U(1)]^2$ is known as the parafermion (PF) one with the central charge $c = 6/5$.¹³ Thus, the energy spectra for the free Hamiltonian are written as

$$E^0 = \frac{\pi v_F}{l} \left[\frac{Q^2}{12} + \frac{j(j+1)}{5} + \frac{\bar{\mathcal{R}}^2}{4} + \Delta + \text{integer} \right], \quad (19)$$

where $\bar{\mathcal{R}}^2 \equiv \bar{T}^2 + \bar{Q}^2$ and Δ is the dimension of the primary fields in the PF sector (see the caption in Table I). Equations (15) and (19) give exactly the same spectra. Note that there is O(2) symmetry between \bar{Q} and \bar{T} . Q and $\bar{\mathcal{R}}$ terms in Eq. (19) can be also represented as

$$\frac{Q^2}{12} + \frac{\bar{\mathcal{R}}^2}{4} = \frac{\bar{N}_x^2 + \bar{N}_y^2 + \bar{N}_z^2}{5}, \quad (20)$$

which is symmetric with respect to the orbital indices, as it should be.

Table I and Fig.2(a) show NRG spectra obtained with keeping 10^4 states at each step. We have checked that the results do not change when 10^4 more states are added. We find that the energy eigenvalues E_N at the N th RG step are given by the free spectrum modified by an additional potential scattering in the O(2) sector:

$$E_N \propto \frac{l}{\pi v_F} E^0 \pm g_N \bar{\mathcal{R}}, \quad (21)$$

TABLE I: Quantum numbers, energy, and degeneracy of 128 low-energy states for odd N . In the parafermion (PF) sector, following notations in Ref.¹³, there are eight primary fields: $\{\mathbf{1}, \sigma_\uparrow, \sigma_\downarrow, \sigma_3, \psi_1, \psi_2, \psi_{12}, \rho\}$. σ 's and ψ 's are abbreviated simply as σ and ψ , respectively. Their scaling dimension Δ is indicated in parentheses. The energy is measured from the value of the non-interacting ground states and then scaled appropriately.

Q	j	SU(3)	$\bar{\mathcal{R}}^2$	PF(Δ)	Energy	degeneracy
0	3/2	$\mathbf{1}$	0	$\mathbf{1}(0)$	0	8
0	1/2	$\mathbf{8}$	0	$\rho(3/5)$	0	4
			0	$\rho(3/5)$	0	4
			2	$\sigma(1/10)$	$\pm\sqrt{2}$	12 each
1	1	$\mathbf{3}$	2/3	$\sigma(1/10)$	$\pm\sqrt{2/3}$	9 each
1	0	$\bar{\mathbf{6}}$	8/3	$\mathbf{1}(0)$	$\pm\sqrt{8/3}$	3 each
			2/3	$\psi(1/2)$	$\pm\sqrt{2/3}$	3 each
-1	1	$\bar{\mathbf{3}}$	2/3	$\sigma(1/10)$	$\pm\sqrt{2/3}$	9 each
-1	0	$\mathbf{6}$	8/3	$\mathbf{1}(0)$	$\pm\sqrt{8/3}$	3 each
			2/3	$\psi(1/2)$	$\pm\sqrt{2/3}$	3 each
2	1/2	$\bar{\mathbf{3}}$	2/3	$\sigma(1/10)$	$\pm\sqrt{2/3}$	6 each
-2	1/2	$\mathbf{3}$	2/3	$\sigma(1/10)$	$\pm\sqrt{2/3}$	6 each
3	0	$\mathbf{1}$	0	$\mathbf{1}(0)$	0	2
-3	0	$\mathbf{1}$	0	$\mathbf{1}(0)$	0	2

with g_N constant. Note that this form remains O(2) symmetric and is derived from the free spectra by shifting $\bar{\mathcal{R}} \rightarrow \bar{\mathcal{R}} \pm 2g_N$ in Eq. (19), *i.e.*, just a ‘‘phase shift.’’ The factor \pm indicates unscreened SC as in the Ising Kondo case.¹⁴ We note that the simple ‘‘phase shift’’ leads to PF excitation spectra for $g_N > 0$.

The N th step in the NRG calculation is related to the energy scale $D\Lambda^{-N/2}$ with discretization parameter¹¹ Λ and we set $\Lambda = 3$. Replacing this for D_{eff} in the two-loop expression of g_{eff} , we find $g_N \propto 1/\sqrt{N}$. Indeed, we obtain

$$E_N - E_\infty \propto \pm \frac{1}{\sqrt{N}} \bar{\mathcal{R}}, \quad (22)$$

in the NRG results as shown in Fig.2 (b), which confirms the two-loop results. This $1/\sqrt{N}$ dependence is a clear contrast to $1/N$ dependence in underscreened and ferromagnetic Kondo models.

4. A hidden angular momentum

We have observed that the O(2) symmetry in the orbital space $\mathcal{Q}\text{-}\mathcal{T}$ is preserved in the energy spectrum of the interacting system $g \neq 0$. This holds asymptotically where the bosonization becomes exact in the low-energy limit. We demonstrate this below by explicit calculations.

The O(2) symmetry is related to a *hidden* conserved quantity of angular momentum. This angular momentum is nontrivial and defined in the two dimensional $\mathcal{Q}\text{-}\mathcal{T}$

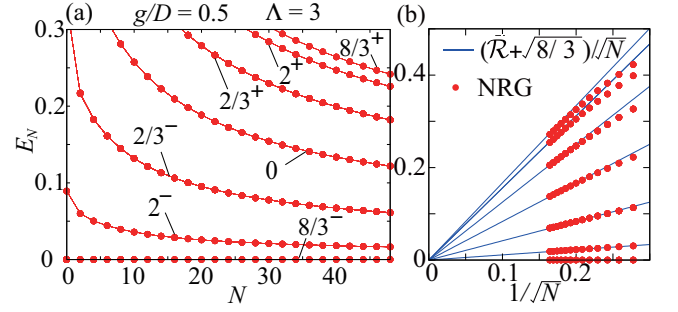


FIG. 2: (color online). (a) NRG spectra for odd N for $g = 0.5D$ and $\Lambda = 3$. At each N , the energy of the lowest-energy states are subtracted. States are labeled by $\bar{\mathcal{R}}^2$ and the sign of the energy listed in Table I. (b) E_N as a function of $1/\sqrt{N}$.

space as

$$\mathcal{L} \equiv \sum_{n \geq 0} \mathcal{L}_n = i \sum_{n > 0} \frac{1}{n} [\mathcal{Q}_n \mathcal{T}_{-n} - \mathcal{T}_n \mathcal{Q}_{-n}] + \mathcal{L}_0. \quad (23)$$

Here, \mathcal{Q}_n and \mathcal{T}_n are the n th Fourier modes for the U(1) bosons and

$$\mathcal{L}_0 = \mathcal{Q}_0 \theta_{\mathcal{T}} - \mathcal{T}_0 \theta_{\mathcal{Q}}, \quad (24)$$

where $\theta_{\mathcal{Q}}(\theta_{\mathcal{T}})$ is a canonical conjugate field to $\mathcal{Q}_0(\mathcal{T}_0)$, with $[\mathcal{Q}_0, \theta_{\mathcal{Q}}] = [\mathcal{T}_0, \theta_{\mathcal{T}}] = i$. \mathcal{L} is conserved for $g = 0$, but is not for $g \neq 0$. The conserved one for $g \neq 0$ is

$$\mathcal{J} \equiv \mathcal{L} + \frac{1}{2} \tau^y, \quad (25)$$

which satisfies $[\mathcal{H}_{\text{int}}, \mathcal{J}] = 0$. We find that eigenvalues of \mathcal{L} are all integers, since $\tilde{S}^y = \sum_{n \geq 0} \tilde{S}_n^y$ with $\tilde{S}_n^y = \frac{1}{2} \mathcal{L}_n$ constituting the SU(2) algebra together with the partners $\tilde{S}^i = \sum_{n \geq 0} \tilde{S}_n^i$ ($i = x, z$), where \tilde{S}_n^i 's are given as

$$\tilde{S}_n^z \equiv \frac{1}{4n} [\mathcal{Q}_n \mathcal{Q}_{-n} - \mathcal{T}_n \mathcal{T}_{-n} + (n \rightarrow -n)], \quad (26)$$

$$\tilde{S}_n^x \equiv \frac{1}{2n} (\mathcal{Q}_n \mathcal{T}_{-n} + \mathcal{T}_n \mathcal{Q}_{-n}), \quad (27)$$

for $n > 0$, and

$$\tilde{S}_0^z \equiv \frac{1}{4} (\mathcal{Q}_0^2 - \mathcal{T}_0^2 + \theta_{\mathcal{Q}}^2 - \theta_{\mathcal{T}}^2), \quad (28)$$

$$\tilde{S}_0^x \equiv \frac{1}{2} (\mathcal{Q}_0 \mathcal{T}_0 + \theta_{\mathcal{Q}} \theta_{\mathcal{T}}). \quad (29)$$

\tilde{S}_n^i 's satisfy $[\tilde{S}_n^i, \tilde{S}_m^j] = i \epsilon^{ijk} \delta_{nm} \tilde{S}_n^k$, and this leads to the SU(2) algebra of $[\tilde{S}^i, \tilde{S}^j] = i \epsilon^{ijk} \tilde{S}^k$. Thus, the eigenvalues of \mathcal{L} are all integer, and \mathcal{L} is, indeed, the ‘‘orbital’’ angular momentum. From this, the eigenvalues of \mathcal{J} should be all half integers. Noticing that the total Hamiltonian is invariant under $\mathcal{J} \rightarrow -\mathcal{J}$, *e.g.*, $\uparrow \leftrightarrow \downarrow$ and $\mathcal{Q} \rightarrow -\mathcal{Q}$, all the energy eigenstates should be degenerate, which is the direct consequence of the unscreened state.

B. Fermi liquid phase

For $T_K \gg J$, the situation is conventional and the ground state is a FL. Each d -electron spin forms a spin singlet with conduction electrons. This phase is continuously connected to the ground state of the spin $S = 2$ four-channel Kondo problem. The way of fully screened processes are similar to those in a Kondo singlet phase in the two-impurity Kondo model, where it is essentially an $S = 1$ two-channel model.¹ Since there is an asymmetry between A_1 and T_2 orbitals in Eq. (2), screening takes place in two stages as T decreases. Indeed, we have confirmed the Fermi liquid properties by using Monte Carlo simulation as is explained in the next section.

IV. CONTINUOUS-TIME QUANTUM MONTE CARLO ANALYSIS

Now, we unveil the NFL properties and determine the global phase diagram of this model by using CTQMC.¹⁵ All the data presented below are for $U = -2\epsilon = 1.5D$, $t = 0.2D$, and $k_F a = 3$. With these values, J is dominated by the superexchange $\sim 4t^2/U$ with a small antiferromagnetic contribution of the RKKY term. For other values of $k_F a$, the results are qualitatively the same as long as J is antiferromagnetic.

A. Thermodynamics

Figure 3(a) shows the susceptibility of local pseudospin χ_{zz} for several values of V . For $V \lesssim 0.275D$, the chirality exhibits unscreened behaviors $\chi_{zz} \sim T^{-1}$ at low T , which is consistent with the discussions above. For larger V , $T_K \gg J$, and thus the ground state is a FL. There, χ_{zz} is small and constant at low T . Figure 3(b) shows that the double occupancy $\langle n_{1\uparrow} n_{1\downarrow} \rangle \sim 1/2 - 2\langle S_1^z S_2^z \rangle$ increases as V increases. This implies that the d electrons become more itinerant as V increases. The intersite spin correlation $\langle S_1^z S_2^z \rangle$ is large and antiferromagnetic for small V , while it is suppressed for large V . As for local configurations in the four-electron sector, the occupancy of the ground-state doublet E with spin $S = 0$ decreases with increasing V , while those for the first and the second excited states $T_2 (S = 1)$ and $A_1 (S = 2)$ increase as shown in Fig.3(c). This is a natural consequence of the Kondo screening, which mixes local configurations with different S .

B. Single-electron dynamics

A drastic change also appears in the single-electron dynamics upon varying V . Figure 4(a) shows the imaginary part of the electron self-energy $\Sigma(i\omega_n)$ for the impurity T_2 orbital, for $T = 0.005D$ as a function of the Matsubara frequency ω_n . For large $V > V^* \simeq 0.3D$, $\text{Im}\Sigma(i\omega_n)$ is linear in ω_n for small ω_n , as expected for the FL state.

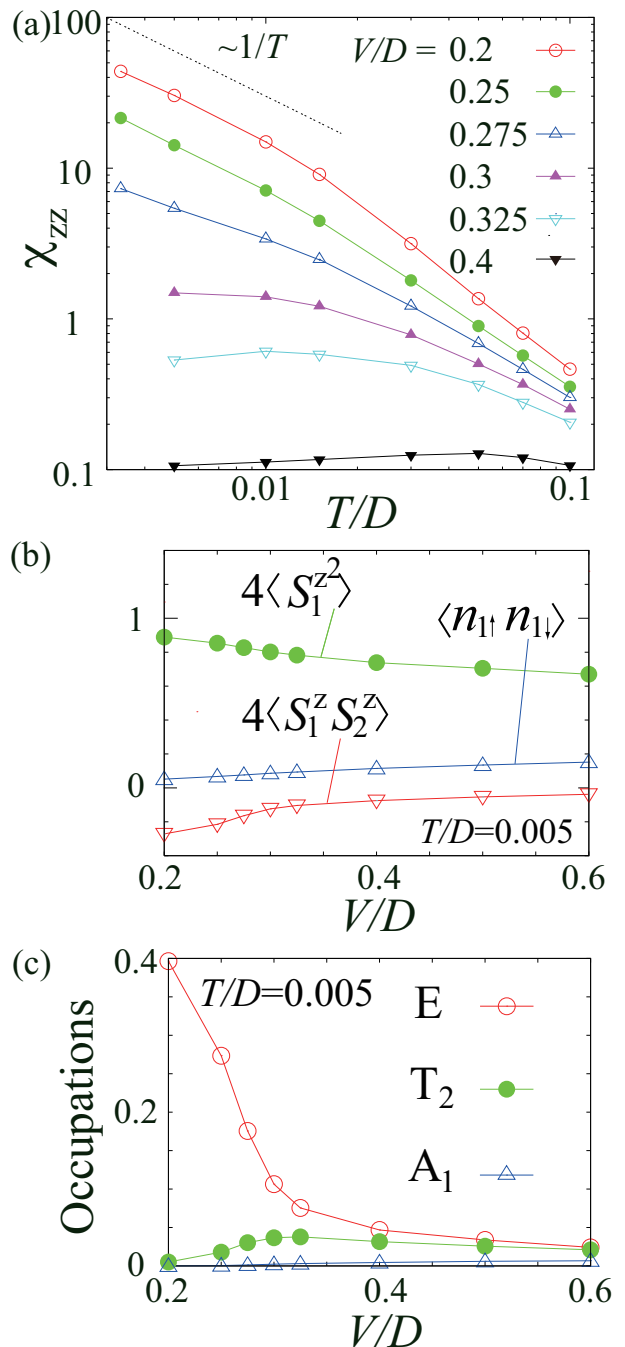


FIG. 3: (Color online). (a) T dependence of susceptibilities χ_{zz} for $V/D = 0.2 - 0.4$, $U = -2\epsilon = 1.5D$, and $t = 0.2D$. (b) Equal-time correlation functions: $\langle S_1^z S_2^z \rangle$, $\langle n_{1\uparrow} n_{1\downarrow} \rangle$, and $\langle S_1^z \rangle$. (c) V dependence of the occupancies of the E , T_2 and A_1 states (per spin and orbital) in the four-electron sector.

For smaller V , it shows a diverging behavior instead and this indicates that the T_2 electrons are localized in the unscreened SC state. This is consistent with our conclusion based on the exchange model (7), since the localization of the T_2 electron leads to the absence of resonance peak at

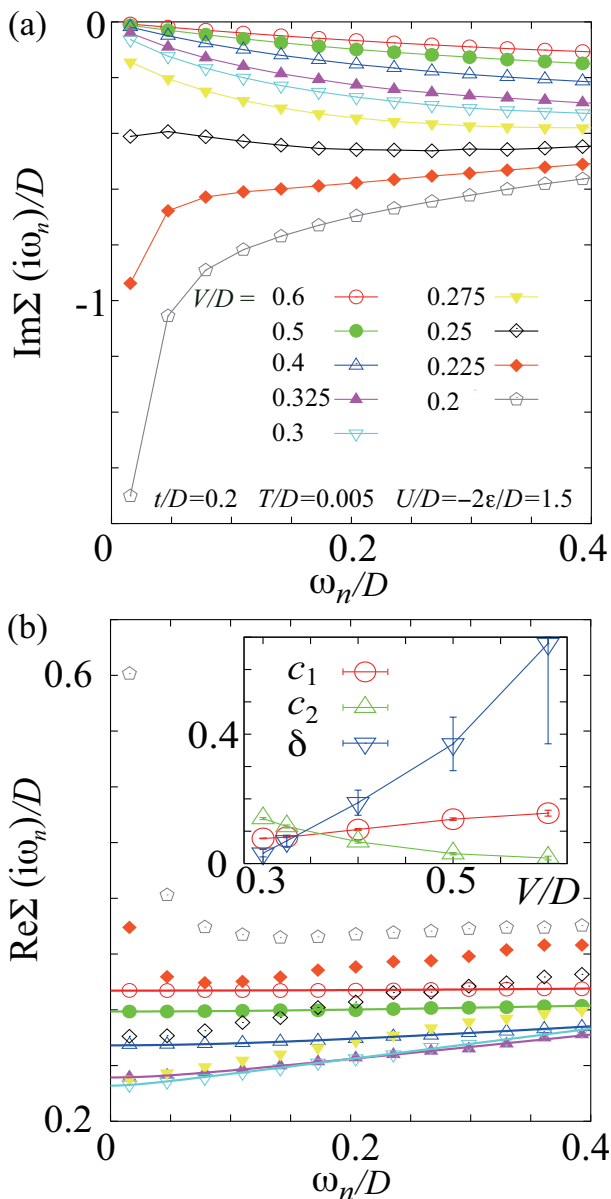


FIG. 4: (Color online). ω_n dependences of (a) $\text{Im}\Sigma(i\omega_n)$ and (b) $\text{Re}\Sigma(i\omega_n)$ for $T = 0.005D$. Lines for $V \geq 0.3D$ in panel (b) represent fit by $c_1 + c_2\sqrt{\delta^2 + \omega_n^2}$ and the values of c_1 , c_2 , and δ are shown in the inset.

the Fermi level in the conduction-electron Green's function for the exchange model (7). The crossover around V^* is similar to that near a critical end point of metal-insulator transitions in strongly correlated systems, *e.g.*, Mott's transition.¹⁶

The real part $\text{Re}\Sigma(i\omega_n)$ shows an even more peculiar behavior near V^* as shown in Fig.4(b). $\text{Re}\Sigma(i\omega_n)$ for $V \sim V^*$ shows a nonanalytic behavior, $\sim c_1 + c_2|\omega_n|$, where c_1 and c_2 are constants. The ω_n dependence for

$V \geq V^*$ is well fitted by $\sim c_1 + c_2\sqrt{\delta^2 + \omega_n^2}$ with $\delta > 0$. As shown in the inset, the critical point is realized by $\delta \rightarrow 0$. This ω_n dependence leads to the NFL form of the retarded self-energy:

$$-\text{Im}\Sigma^R(\omega) \sim |\omega|, \quad (30)$$

which is the same as in the marginal FL theory.¹⁷ The NFL point $V^* \sim 0.3D$ is consistent with the transition point of V in Fig.3. Thus, our CTQMC results for finite temperatures strongly suggest that there is a quantum critical point separating the FL and the unscreened phases at $T = 0$.

As for the A_1 electron, the imaginary part of the self-energy shows FL behavior for all the values of V we examined. This persists for smaller t and is related to the fact that the A_1 orbital cannot interact with the non-magnetic E doublet apart from potential scattering.

This NFL is stable against various perturbations which are relevant at some other types of critical points. For example, it is stable against magnetic field and particle-hole asymmetry, and this is understood from the difference in the ground-state entropy in the two stable phases. Distortion that breaks the T_d symmetry may give nontrivial effects on the stability of the NFL. Examination of the stability of the NFL against distortions and clarifying the NFL finite-size spectra are our future work.

V. SUMMARY

We have investigated an Anderson model with four impurities on a regular tetrahedron. We have found that the system has two stable fixed points. One is the new fixed point where an emergent SC of the tetrahedron is not screened by conduction electrons for small V with diverging effective mass and the emergent PF excitations, and is a new class of singular FL states. The other is a Kondo screened FL state for large V . Our CTQMC results have revealed that the new critical NFL state appears, accompanying the d -electron localization transition at zero temperature and the self-energy exhibits marginal FL-like frequency dependence.

Acknowledgment

The authors thank H. Kusunose and J. Otsuki for their advice on Monte Carlo codes. This work is supported by KAKENHI (Grants No. 19052003 and No. 30456199) and by the Next Generation Super Computing Project, Nanoscience Program, from the MEXT of Japan. A part of the numerical calculations was done at the Supercomputer Center at the ISSP, University of Tokyo.

-
- ¹ B. A. Jones, and C. M. Varma, Phys. Rev. Lett. **58**, 843 (1987), I. Affleck, A. W. W. Ludwig, and B. A. Jones, Phys. Rev. B **52**, 9528 (1995).
- ² H. v. Löhneysen, A. Rosch, M. Vojta, and P. Wölfle, Rev. Mod. Phys. **79**, 1015 (2007).
- ³ For overview see, *Introduction to Frustrated Magnetism*, edited by C. Lacroix and F. Mila, (Springer Verlag, Berlin, 2010).
- ⁴ T. Jamneala, V. Madhavan, and M. F. Crommie, Phys. Rev. Lett. **87**, 256804 (2001).
- ⁵ K. Ingersent, A. W. W. Ludwig, and I. Affleck, Phys. Rev. Lett. **95**, 257204 (2005).
- ⁶ V. V. Savkin, A. N. Rubtsov, M. I. Katsnelson, and A. I. Lichtenstein, Phys. Rev. Lett. **94**, 026402 (2005).
- ⁷ B. Lazarovits, P. Simon, G. Zarand, and L. Szunyogh, Phys. Rev. Lett. **95**, 077202 (2005).
- ⁸ H. Tsunetsugu, J. Phys. Soc. Jpn. **70**, 640 (2000); Phys. Rev. B **65**, 024415 (2001).
- ⁹ D. L. Cox, Phys. Rev. Lett. **59**, 1240 (1987).
- ¹⁰ P. Coleman and C. Pépin, Phys. Rev. B **68**, 220405(R) (2003), P. Mehta, N. Andrei, P. Coleman, L. Borda, and G. Zarand, Phys. Rev. B **72**, 014430 (2005).
- ¹¹ K. G. Wilson, Rev. Mod. Phys. **47**, 773 (1975).
- ¹² I. Affleck and A. W. W. Ludwig, Nucl. Phys. B **360**, 641 (1991).
- ¹³ E. Ardonne, J. Phys. A: Math. Gen. **35**, 447 (2002).
- ¹⁴ P. W. Anderson, J. Phys. C **3**, 2436 (1970).
- ¹⁵ P. Werner, A. Comanac, L. de' Medici, M. Troyer, and A. J. Millis, Phys. Rev. Lett. **97**, 076405 (2006).
- ¹⁶ M. Imada, A. Fujimori, and Y. Tokura, Rev. Mod. Phys. **70**, 1039 (1998).
- ¹⁷ C. M. Varma, P. B. Littlewood, S. Schmitt-Rink, E. Abrahams, and A. E. Ruckenstein, Phys. Rev. Lett. **63**, 1996 (1989).